Scientia Iranica D (2015) 22(6), 2482–2491

Sharif University of Technology
Scientia Iranica
Transactions D: Computer Science & Engineering and Electrical Engineering
www.scientiairanica.com

Analytical quasi 3D modeling of an axial flux PM motor with static eccentricity fault

K. Abbaszadeh* **and A. Rahimi**

Department of Electrical Engineering, K. N. Toosi University of Technology, Tehran, Iran.

Received 28 October 2014; received in revised form 25 April 2015; accepted 5 September 2015

KEYWORDS
Axial flux permanent magnet machine;
Static eccentricity;
Unbalanced magnetic forces;
Analytical quasi 3D modeling.

Abstract. In this paper, an analytical quasi three-dimensional (3D) analysis is used to model an Axial Flux Permanent Magnet Motor (AFPMM) with Static Eccentricity (SE) fault. Due to AFPMMs' inherent 3D geometry, accurate modeling of AFPMMs requires 3D Finite Element Analysis (FEA). However, 3D FEA is generally too time consuming. The proposed analytical quasi 3D modeling method gives the ability to reduce the time and size of computations by transforming 3D geometry of an AFPMM to several two-dimensional (2D) models, then treating each of the 2D models as a linear machine. Using quasi 3D modeling, the air-gap length variation, magnetic flux density, and magnetic forces are modeled in an AFPMM with SE fault by analytical approaches. The results given by the proposed method are compared with 3D FEA results and it is shown that these results are accurate enough to model the AFPMM with SE fault correctly. Moreover, using this method is a significantly less time consuming process than 3D FEA simulation process, which is a great advantage of this method. Finally an experimental validation using two test coils on stator teeth has been carried out to show accuracy of the simulation results of the proposed method.

1. Introduction

Nowadays, Axial Flux Permanent Magnet Machines (AFPMMs) have been widely investigated for various applications due to their compact structure, high efficiency, and high torque density [1,2]. These machines are very attractive for applications, such as light electric traction or elevation [3] and Electric Vehicles (EVs) [4] in which the axial length of the machine is a limiting design parameter and direct coupling is desirable.

Due to the specific structure of AFPMMs and use of high energy density permanent magnet materials, great axial forces are produced between rotor magnets and stator teeth during machine performance and even when the stator windings are not excited. In the healthy condition, in which air-gap length is symmetric, these forces are perpendicular to the shaft axis with uniform distribution, so axial forces do not affect the performance of AFPMMs. However, under eccentricity condition, where the rotor is inclined and the air-gap length is asymmetric, the axial forces become unbalanced and produce Uneven Magnetic Forces (UMFs) [5,6]. These UMFs are important, because they can result in vibration and acoustic noise during machine performance and reduce lifetime of the bearings. Therefore, it is necessary to model and simulate the machine with eccentricity fault in order to predict or diagnose the machine characteristics in the faulty condition. There are few publications which have studied eccentricity in AFPMMs. In [6,7] the authors proposed a new definition for Static Eccentricity (SE) fault and continued their work on detection of this fault in [8].

Modeling an AFPMM can be done via analytical

*. *Corresponding author. Tel.: +98 21 84062324;*
E-mail address: abbaszadeh@kntu.ac.ir (K. Abbaszadeh)

methods [9,10], Magnetic Equivalent Circuit (MEC) method [4,11], two-dimensional (2D) [12], and three-dimensional (3D) Finite Element Analysis (FEA) [13], or a combination of these methods [14,15]. Precise modeling of an AFPMM under eccentricity condition requires accurate computation of machine characteristics, especially in the air-gap region of the machine. Besides, AFPMMs have inherent 3D geometry from the modeling point of view. The most accurate solution for modeling the machine in this condition is 3D FEA. However, this method is highly time consuming. Thus, some literature proposed alternative methods to reduce the 3D geometry of the axial flux machine in a 2D plane; generally, they model the axial machines in the average radius plane of machine and treat it like a linear machine using 2D FEA, MEC method, or analytical equations [16,17]. Although this method is much faster than 3D FEA, for some proposes like computing cogging torque, eddy current loss, and force computation, this method is not accurate enough, because it does not consider variation of teeth and magnet length along the machine radius. Another possible solution appearing in the literature, which is known as the quasi 3D method [18,19], consists in carrying out 2D FEA simulations or analytical modeling in different planes along the radius of the axial machine. Thus, an axial machine is considered to be composed of several individual linear machines, and computations for each plane are done separately. Then, the overall performance of machine is obtained by summing the performances of these linear machines. The more the planes are used, the more accurate the results are. Thus, it must be considered that the time consumption of these simulations is directly proportional to the number of chosen planes. It is also possible to find axial flux machine modeling with the combination of 2D FEA and analytical tools in order to reduce the computation time in comparison with 3D FEA [16].

This paper proposes a quasi 3D analytical method to model an AFPMM with SE fault. The main advantage of the proposed method is the saving time of computations in comparison with the 3D FEA. Moreover, with sufficient number of computation planes, it is shown that the accuracy of results is acceptable. Results given by the presented quasi 3D method are validated by comparing the results of the proposed method with those obtained by 2D and 3D FEA simulations. Also, an experimental validation has been carried out to show the accuracy of the proposed method models.

2. Analytical quasi 3D modeling of an AFPMM

In order to model an AFPMM using analytical or 2D FEA analysis, usually, a specific radius of the machine

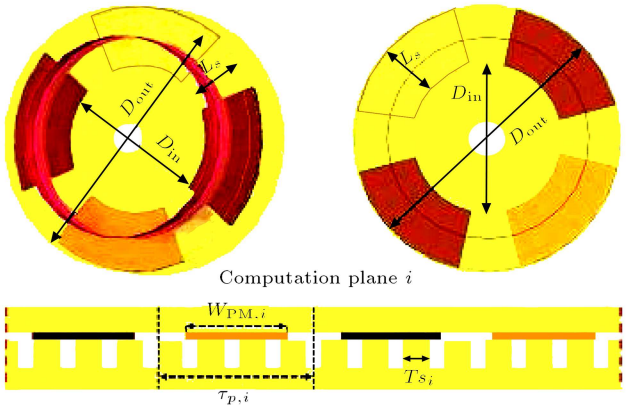

Figure 1. Selecting computation plane i.

in a 2D plane is selected and then the whole machine is treated like a linear machine as illustrated in Figure 1. Generally, this layer is selected in the mean radius of the machine. Pole pitch and the pole shoe width to pole pitch ratio for the selected plane can be obtained by:

$$\tau_{p,i} = \frac{\pi D_{\text{ave},i}}{2p}, \tag{1}$$

$$\alpha_{p,i} = \frac{w_{\text{PM},i}}{\tau_{p,i}}, \tag{2}$$

where w_{PM} is length of the rotor magnets and D_{ave} is the average diameter of the selected plane.

The first step of modeling a rotating electrical machine is calculation of the air-gap flux density. All other characteristics that explain the machine performance, such as torque, winding induced voltages, forces, etc., can be derived from air-gap magnetic flux density waveform. Thus, if the air-gap flux density is modeled accurately, other characteristics of the machine also can be calculated more accurately.

2.1. Air-gap flux density distribution

An equation for calculating air-gap flux density of a radial permanent magnet machine is given in Box I [20], which is reformed in Cartesian coordinates for use in linear permanent magnet machines as [21], where g_e is the effective air-gap length, B_r is the remanence flux density of the PM material, μ_0 is the free space coil permeability, μ_{PM} is the PM recoil permeability, and h_{PM} is the magnet height.

The flux density distribution in each selected plane can be calculated from Eq. (3) shown in Box I.as In this equation, stator slots effects on air-gap flux density are not considered. The slotting effect can be described by a change of permeance according to the flux path passing through the air-gap as described in [21]. Figures 2 and 3 show flux density distribution computed by Eq. (3) with considering stator slotting effects, 2D and 3D FEA in the mean radius of the machine for a 4-pole AFPMM with 15 stator slots. Table 1 shows the modeled AFPMM specifications.

$$\vec{B}_{\mathrm{PM},i}(x) = -\sum_{n=1,3,5,\cdots}^{\infty} \frac{\frac{8B_r}{n\pi}\sin\left[\frac{\alpha_{p,i}n\pi}{2}\right]}{\left(e^{-\frac{2n\pi g_e}{\tau_{p,i}}}+1\right)+\frac{\mu_{\mathrm{PM}}\left(-e^{-\frac{2n\pi g_e}{\tau_{p,i}}}+1\right)\left(e^{\frac{2n\pi h_{\mathrm{PM}}}{\tau_{p,i}}}+1\right)}{\mu_0\left(e^{\frac{2n\pi h_{\mathrm{PM}}}{\tau_{p,i}}}-1\right)}} \times e^{-\frac{2n\pi g_e}{\tau_{p,i}}}\cos\left(\frac{n\pi x}{\tau_{p,i}}\right) \quad (3)$$

Box I

Table 1. Machine specifications.

Parameter	Definition	Value
p	Number of poles	4
g_0	Physical length of air-gap under healthy condition	1.5 mm
h_{PM}	Thickness of PM	5 mm
D_{out}	Stator outer diameter	158 mm
D_{in}	Stator inner diameter	88.5 mm
B_r	Remanence flux density of the PM material	1.0 T
μ_{PM}	Relative permeability of PM material	1.05

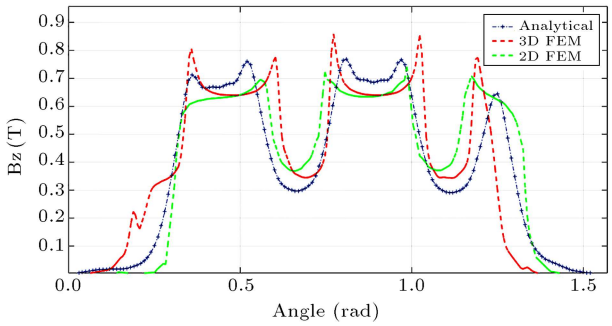

Figure 2. Air-gap magnetic flux density under one-pole pitch.

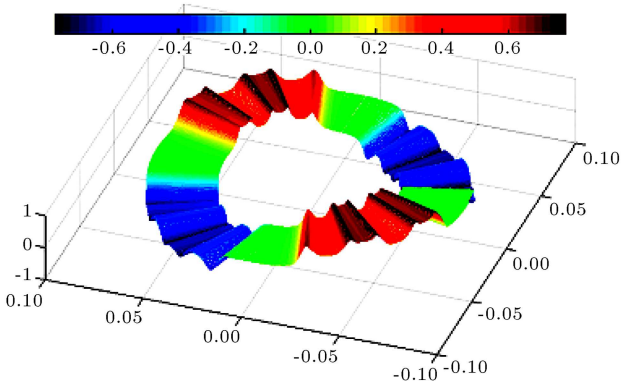

Figure 3. Air-gap magnetic flux density distribution in 40 layers.

The modeled machine is a TORUS-S type machine that was designed and built for EV applications [22,23]. The TORUS-S structure from magnetic point of view can be considered as a composition of two separate identical single rotor-single stator AFPMMs which can be modeled individually. Hence, only one side of this machine is modeled to reduce the computation size and simulation time.

Using mean radius only as a computation plane for modeling may give proper results in AFPMMs that their magnet-length to pole-pitch ratio is constant along the machine radius. But without considering the stator teeth variations and different rotor magnet shapes, the results are not accurate enough for computing some machine characteristics which are highly dependent on the shape of teeth and magnets, such as cogging torque, forces, and eddy current loss. To improve the accuracy of results, the number of computation planes should be increased. Thus, in analytical quasi 3D method, an AFPMM is considered to be composed of several individual linear machines in different radii of the AFPMM, and computations for each plane are done separately. Then, the overall performance of the machine is obtained by summing the performances of these linear machines. Although the simulation time will increase proportionally by increase in the number of computation planes, this increase is negligible in comparison with the high time consuming process of 3D FEA. By using quasi 3D method, the variations of the shape of magnets and stator teeth along the machine radius are considered in the computation results. The radius of a particular computation plane i, starting from internal diameter of the machine, is given by:

$$r_i = \left(D_{\mathrm{in}} + j\frac{L_s}{N}\right)/2, \quad (4)$$

where D_{in} is the internal diameter of the stator, N is the number of computation planes, $j = 2i-1$ ($j = 1,3,5\cdots$), and L_s are the total length of the stator. It is defined as:

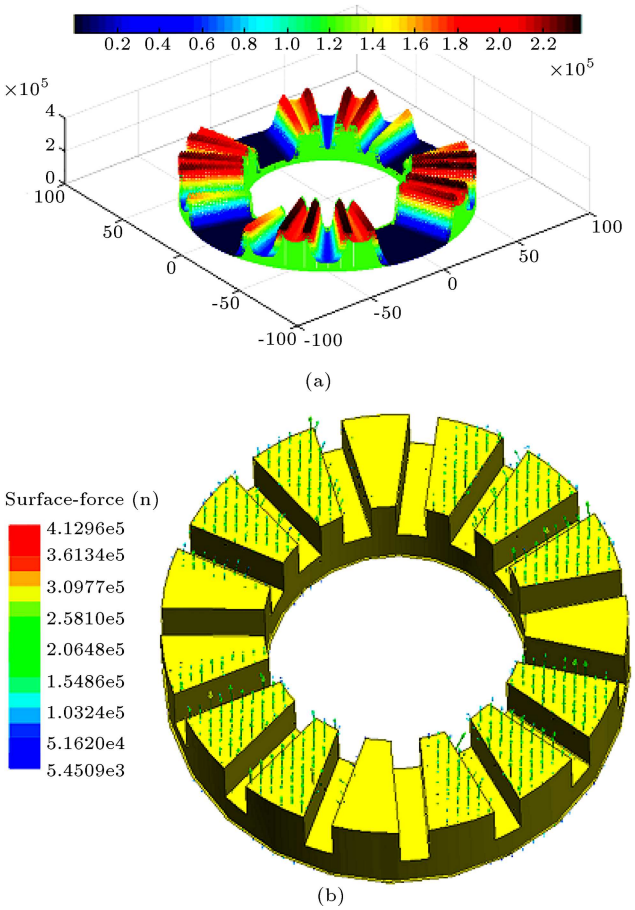

Figure 4. Force density on stator surface: (a) Quasi 3D analytical modeling; and (b) 3D FEA modeling.

$$L_s = \frac{D_{\text{out}} - D_{\text{in}}}{2}, \tag{5}$$

where D_{out} is the external diameter of the axial flux machine stator.

Figure 4 shows the air-gap flux density computed in 40 computation layers along the machine radius using analytical quasi 3D method. The variation of magnetic shapes and effects of stator teeth on flux density distribution is obviously shown. Moreover, this should be noted that quasi 3D approach allows taking into account different magnet shapes and variation of tooth width in the direction of machine radius [10,18]. Although the end winding effect in this study is not considered, it is shown that the influence of this on the accuracy of results is not significant and the difference between modeling results and experimental measurements is negligible.

2.2. Analytical quasi 3D force calculation

In order to calculate the unbalanced axial forces in an AFPMM with eccentricity fault analytically, Maxwell stress method is used [24]:

$$\vec{f} = \nabla.\tau. \tag{6}$$

$\vec{f}$ is the force density, and τ is the Maxwell stress tensor. Maxwell stress tensor is defined as follows:

$$\tau_{i,j} = \frac{B_i B_j}{\mu_0} - \delta_{i,j}\frac{|B|^2}{2\mu_0}, \tag{7}$$

where $\vec{B}$ is the magnetic flux density, $\vec{i}$ and $\vec{j}$ are unit vectors of the specific coordinate system, and $\delta_{i,j}$ is the Kroner's delta function.

The total force is obtained by integrating force density in the object volume.

$$\vec{F} = \int_V \nabla.\tau dv, \tag{8}$$

where V is the volume of the object.

Using Gauss theorem, Eq. (12) can be rewritten as follow:

$$\vec{F} = \oint_S \tau.\vec{n} ds, \tag{9}$$

where $\vec{n}$ is the rotor axis unit vector which is parallel to the magnetic flux direction. And S is the surface of the object.

Magnetic flux density can be resolved into two orthogonal components: B_n which is normal to the boundary S, and B_t which is tangential to the boundary S. Thus, the magnetic flux density vector becomes:

$$\vec{B} = B_n\vec{n} + B_t\vec{t}. \tag{10}$$

Here, t is the unit-vector tangential to the boundary S.

Expression (9) can now be rewritten as:

$$\vec{F} = \oint_S \left(\frac{1}{\mu}(B_n^2 - B_t^2)\vec{n} - \frac{1}{2\mu_0}B_n B_t\vec{t}\right) ds. \tag{11}$$

For 2D analysis of an electrical machine, Eq. (10) can also be written in another form, wherein the surface integral is reduced to the line integral:

$$\vec{F} = l_e r \int_0^{2\pi} \left(\frac{1}{2\mu_0}(B_n^2 - B_t^2)\vec{n} + \frac{1}{\mu_0}B_n B_t\vec{t}\right) d\theta. \tag{12}$$

Here, r is radius of the integration contour.

In quasi 3D modeling of an AFPMM, geometry of the machine is reduced in several 2D planes and most of the air-gap flux in each individual plane is considered to be parallel to rotor axis. So it is assumed that the normal magnetic flux density component is significantly larger than the tangential one and the latter is, therefore, ignored. Thus, Eq. (12) can be simplified for each computation plane:

$$\vec{F}_i = \frac{L_s r_i}{2\mu_0}\int_0^{2\pi} B_{n,i}^2\vec{n}d\theta. \tag{13}$$

The total force for the whole machine is then computed

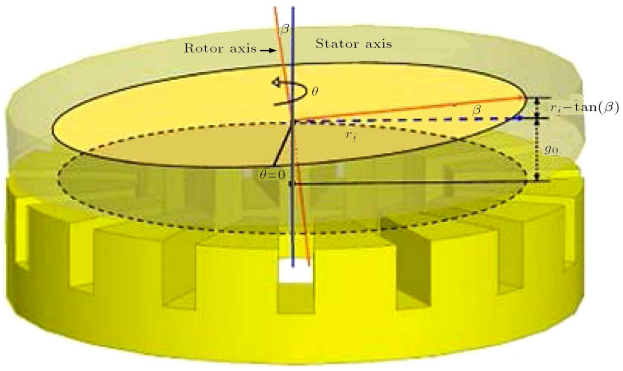

Figure 5. An AFPMM under eccentricity condition.

as:

$$\vec{F} = \sum_{i=1}^{N} \vec{F}_i. \tag{14}$$

Figure 4 shows the force density distribution on stator surface computed in 20 computation planes along the machine radius using the proposed method and force density computed from 3D FEA. It is shown that the results given by the analytical quasi 3D method are almost similar to 3D FEA simulation results, however time of computations in the proposed method was significantly less than that of 3D FEA.

3. Effects of static eccentricity on machine characteristics

Figure 5 shows an AFPMM under SE condition. In the healthy condition, air-gap length is uniform around the shaft axis. So the air-gap length is a constant value:

$$g = g_0. \tag{15}$$

In an AFPMM with SE fault, rotor shaft of the machine is inclined so that the stator and rotor axes do not coincide and the rotor rotates around its shaft. In this condition, air-gap length is uniform around the machine and the air-gap minimum and maximum are fixed in the space. In this condition, the length of gaps between rotor magnets and stator teeth in one half of the motor (i.e., the left side in Figure 5) is reduced, while rising in the other half. Thus, the air-gap length can be expressed as:

$$g = g_0 + r_i \tan\beta \sin\theta, \tag{16}$$

where β is the inclination angle, and θ is the rotational position of the rotor from the reference position:

$$\theta = \omega t + \theta_0, \tag{17}$$

where ω is the angular velocity of the rotor.

Eq. (16) describes the air-gap length of an AFPMM with SE fault. So, replacing Eq. (16) in Eq. (3) gives the air-gap flux density distribution of the modeled AFPMM under SE condition.

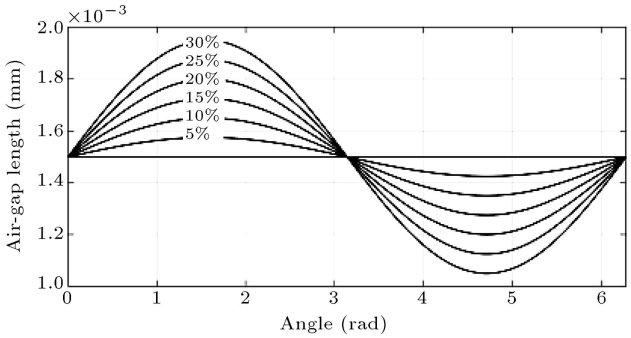

Figure 6. Air-gap length for different SEF%.

As described in [6], in SE condition, β has a constant value. Although in Eq. (15), g varies with θ, the value of g, for each position of rotor, is fixed. Figure 6 shows the air-gap length variation in the mean radius of the investigated AFPMM with respect to θ under different Static Eccentricity Factor (SEF) percentages. SEF for each calculation plane is defined as follows:

$$\text{SEF}_i = \frac{r_i \tan(\beta)}{g_0} \times 100\%. \tag{18}$$

3.1. Effects of static eccentricity on air-gap flux density

The air-gap flux distribution is one of the most important characteristics in electrical machines, because any changes in this feature will affect other characteristics of the machine. Figure 7 shows the flux density waveform of the machine in different SEFs. It is shown that the eccentricity fault clearly affects the air-gap flux pattern of the AFPMM.

The flux path reluctance is directly proportional to the length of the air-gap. Considering Figure 5 as the eccentricity condition of the machine, in the left side of the machine, the air-gap length is minimum and in right side of the machine, the air-gap length is maximum. This leads to the creation of low reluctance flux paths in the left side of the machine and consequently increasing of the air-gap flux density in this part.

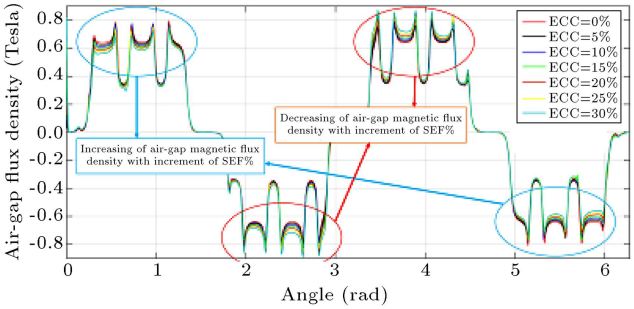

Figure 7. Air-gap flux density variation with increment of SEF%.

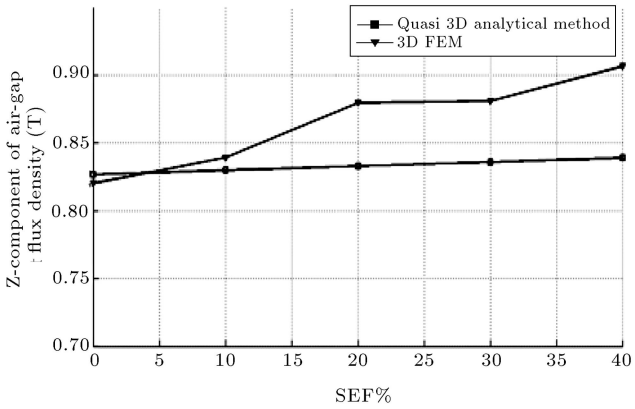

Figure 8. Maximum values of air-gap flux density.

In the other half of the motor (the right side in Figure 5), the air-gap length is increased. So the air-gap flux density is reduced. Figure 7 obviously shows these changes. Moreover, Figure 8 shows the increase in maximum flux density with increase in the SEF due to the reduction of air-gap length in the left side of the machine. One more thing that should be noted is that for the worst SEF condition (here 40%), the maximum of the air-gap flux density did not exceed 0.9 T. So the machine stator and rotor steel are not in saturation. Therefore, the analytical quasi 3D computation, which is used for modeling the machine without considering the saturation effects, is reasonable.

3.2. Unbalanced magnetic forces

Figure 9 shows the calculated total force between rotor and stator of the machine under different SEFs in comparison with the proposed analytical quasi 3D method and 3D FEA simulation. Although eccentricity distorts the flux distribution of the air-gap, as it was expected, there are no significant changes in the total force with increment of SEF, because the decrement of air-gap length in the left side of the machine is equal to its increment in the right side. Consequently, increment of forces in the right side of the machine is expected to be approximately equal to the decrement of forces in the left side.

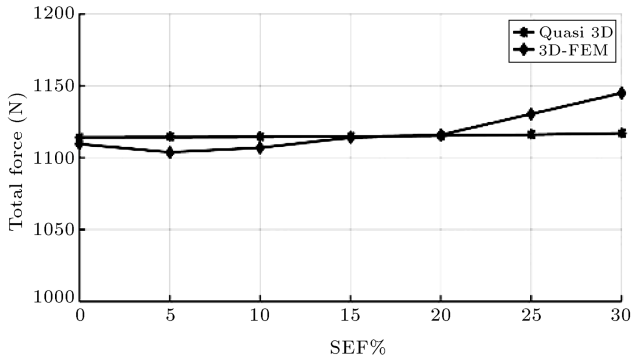

Figure 9. Total magnetic forces.

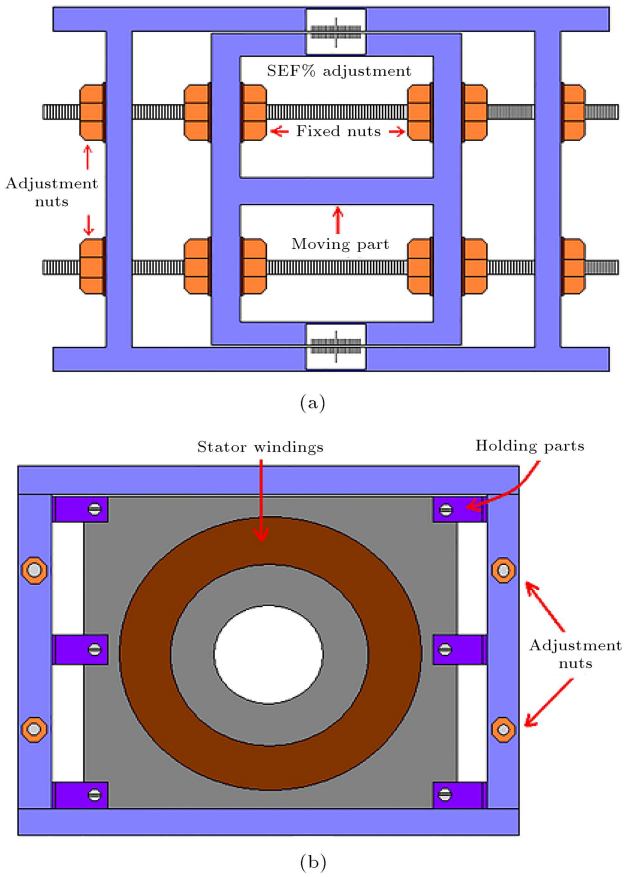

Figure 10. The designed frame for studying SE fault: (a) Front view; and (b) side view.

4. Experimental validation

In order to validate the results of the proposed method, a mechanism was designed and applied to study SE with different SEFs on the modeled AFPMM's test bed. To have faulty machine, rotor of the AFPMM is mounted on a frame, which can rotate in several degrees as shown in Figure 10.

Different SEFs condition simulated and measurements are compared with the modeled faulty machine. Figure 11 shows the test bed of the machine with the designed mechanism, which was used for obtaining the experimental results given for validation of the simulation results.

4.1. Back EMF voltage

In order to validate the proposed method for modeling the AFPMM with SE fault, first, the back-electromotive force (EMF) of the machine was considered, because it covers the air-gap flux waveform and nonlinearity of materials, and it contains all geometric details of the machine. Figure 12 shows the stator winding coils of the modeled AFPMM.

The no-load phase voltage, produced by the magnets, is only computed by the air-gap flux density distribution for each computation plane as:

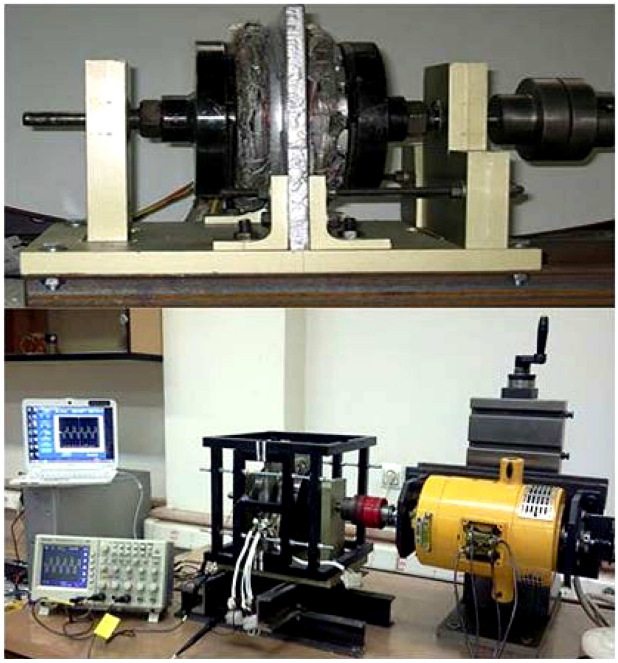

Figure 11. The experimental test bed for studying SE fault.

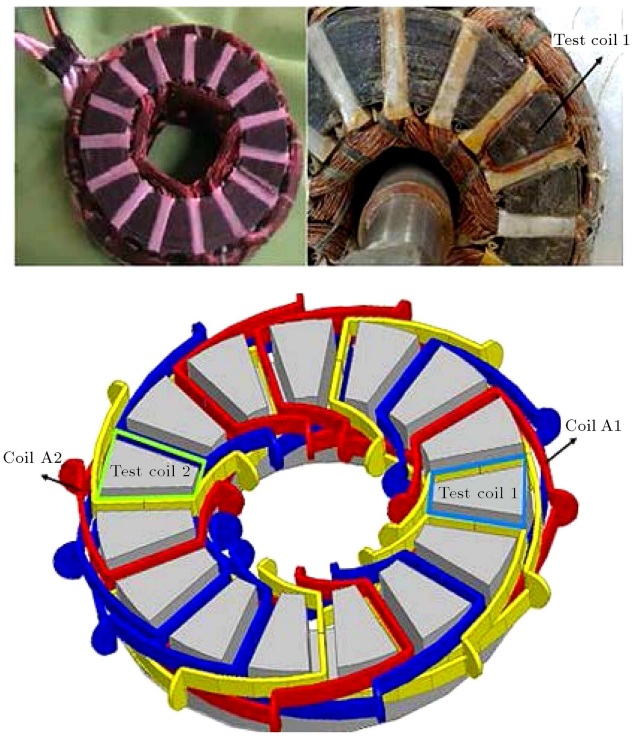

Figure 12. Stator winding coils and the two located test coils.

$$E_i(t) = -N_{ph} k_p \frac{d\phi_i}{dt}, \tag{19}$$

where N_{ph} is the number of coil turns per phase, K_p is the winding factor for the fundamental wave, and ϕ is the air-gap flux which is obtained by numerically integrating the air-gap flux density distribution given by Eq. (3). Induced voltage of each phase is computed by the variation of flux which is the flow through the five coils of each phase by time.

The no-load phase voltage for the whole machine is then computed as:

$$E(t) = \sum_{i=1}^{N} E_i(t). \tag{20}$$

By neglecting the leakage fluxes which mainly flow through tooth tips, a notable difference in the amplitudes of the no-load phase voltages is resulted between the proposed analytical approach and experimental results. So, by considering a leakage factor in the analytical computations, the quasi 3D analytical results are modified. A 3D FEA is used in order to find the correct leakage factor for the modeled AFPMM. In this case, the leakage factor for the modeled machine, obtained by 3D FEA, is 0.93.

It seems that SE is mostly affected by the voltages induced in the phases which their coils are located against the maximum and minimum of air gap length (in this case, it is phase A shown in Figure 12).

Five coils of phase A winding are demonstrated in Figure 12. Regarding previous assumption, coils A1 and A2 are placed at maximum and minimum air-gap lengths. Thus, these coils are mostly affected by the eccentricity among all of the phase A coils. Simulations show that the increase in the induced voltage of coil A2 with eccentricity is approximately equal to the decrease in the induced voltage of coil A1. Therefore, the back-EMF of phase A, that is the summation of the induced voltage of phase A coils, is not a suitable characteristic for describing the effects of eccentricity on the AFPMM performance. Figure 13 shows the phase A no-load induced voltage in the healthy condition and with SEF 30%. There is no individual access to the phase coils for measuring the induced voltage of each coil and, as it was explained before, it is difficult to accurately examine the eccentricity effects on phase no-load phase voltages. Therefore, an alternative method is used in order to show the effects of eccentricity on the modeled AFPMM.

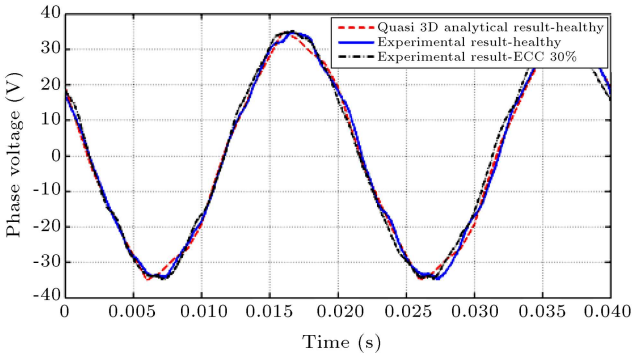

Figure 13. Phase A induced voltage.

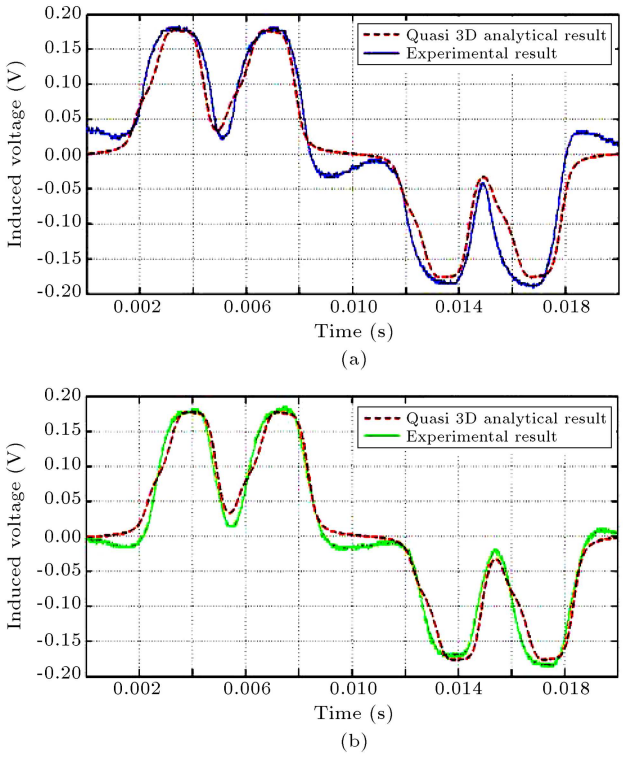

Figure 14. Test coils 1 and 2 induced voltages in healthy condition: (a) Test coil 1; and (b) test coil 2.

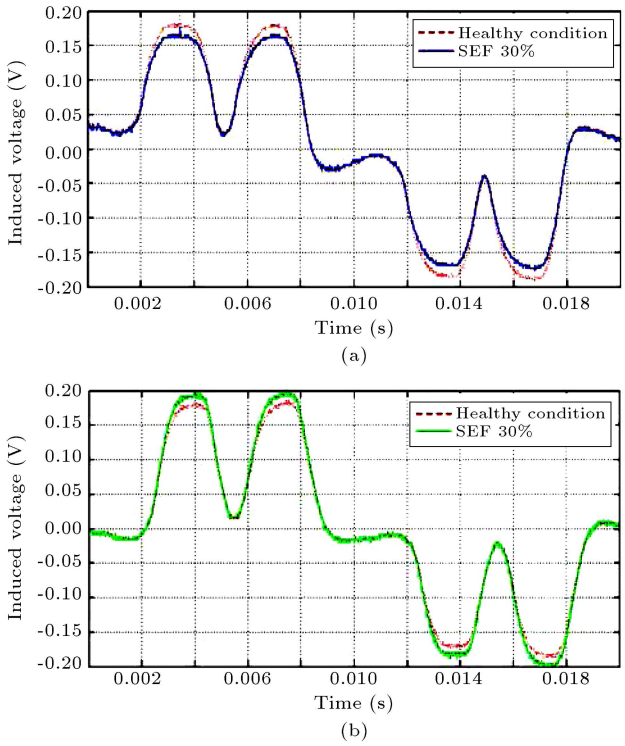

Figure 15. Test coils 1 and 2 induced voltages in SEF 30%: (a) Test coil 1; and (b) test coil 2.

4.2. Test coil voltage

Two test coils were built with 4 coplanar turns and placed on the two teeth that were located against the maximum and minimum air gap length in SE fault condition, as shown in Figure 12 and their induced voltages were measured. Induced voltages of these test coils at nominal speed are obtained from the quasi 3D analytical model and they are compared with the measured one in healthy and eccentric condition of motor with SEF=30%. It is observed that these results have a good agreement, which shows the accuracy of the model. The induced voltages in coil 1 and coil 2 in healthy condition are shown in Figure 14.

Figure 15 shows the effect of eccentricity on the voltage induced in test coil 1 and test coil 2. It is shown that in test coil 1 which is located against the maximum air-gap length, the induced voltage amplitude is decreased and in test coil 2 which is located against the minimum air-gap length, the induced voltage amplitude is increased with eccentricity. Despite back-EMF, the effect of eccentricity on test coils is obvious and the results given have a good agreement with the simulation results of the proposed method.

5. Conclusions

In this paper, an analytical quasi 3D model is presented to model and simulate the effects of static eccentricity in an axial-flux PM machine. In this model, the 3D geometry of the axial-flux PM machine is considered to be composed of several linear machines and each plane computation is computed via analytical equations. The effects of eccentricity on different characteristics of an AFPMM are modeled and presented using the proposed method and the given results are compared with 3D FEA results. It is shown that the simulation results are acceptable in order to model the static eccentricity effects on the magnetic flux density, forces and induced phases voltage in a specific AFPMM. The proposed method is significantly faster than 3D FEA. Finally, an experimental validation, using two test coils on stator teeth, has been carried out to show the accuracy of simulation results of the proposed method.

References

1. Aydin, M., Surong, H. and Lipo, T.A. "Design, analysis, and control of a hybrid field-controlled axial-flux permanent-magnet motor", *IEEE Trans. on Ind. Electron.*, **57**(1), pp. 78-87 (2010).

2. Aydin, M., Surong, H. and Lipo, T.A. "Torque quality and comparison of internal and external rotor axial flux surface-magnet disc machines", *IEEE Trans. on Ind. Electron.*, **53**(3), pp. 822-830 (2006).

3. Ficheux, R.L., Caricchi, F., Crescimbini, F. and Honorati, O. "Axial-flux permanent-magnet motor for

direct-drive elevator systems without machine room", *IEEE Trans. on Ind. Appl.*, **37**(6), pp. 1693-1701 (2001).

4. Saied, S., Abbaszadeh, K. and Fadaie, M. "Reduced order model of developed magnetic equivalent circuit in electrical machine modeling", *IEEE Trans. on Magn.*, **46**(7), pp. 2649-2655 (2010).

5. Rahimi, A. and Abbaszadeh, K. "Quasi 3D modeling of the magnetic forces in axial flux PM machines with rotor eccentricity", *22nd Iranian Conf. on Electr. Eng. (ICEE)*, pp. 585-588, Tehran, Iran (2014).

6. Mirimani, S.M., Vahedi, A. and Marignetti, F. "Effect of inclined static eccentricity fault in single stator-single rotor axial flux permanent magnet machines", *IEEE Trans. on Magn.*, **48**(1), pp. 143-149 (2012).

7. Mirimani, S.M., Vahedi, A., Marignetti, F. and De Santis, E. "Static eccentricity fault detection in single-stator-single-rotor axial-flux permanent-magnet machines", *IEEE Trans. on Ind. Appl.*, **48**(6), pp. 1838-1845 (2012).

8. Mirimani, S.M., Vahedi, A., Marignetti, F. and Di Stefano, R. "An online method for static eccentricity fault detection in axial flux machines", *IEEE Trans. on Ind. Electron.*, **62**(3), pp. 1931-1942 (2015).

9. Chan, T.F., Weimin, W. and Lai, L.L. "Performance of an axial-flux permanent magnet synchronous generator from 3-D finite-element analysis", *IEEE Trans. on Energy Convers.*, **25**(3), pp. 669-676 (2010).

10. Tiegna, H., Amara, Y. and Barakat, G. "A new quasi-3-D analytical model of axial flux permanent magnet machines", *IEEE Trans. on Magn.*, **50**(2), pp. 817-820 (2014).

11. Abbaszadeh, K. and Maroufian, S.S. "Axial flux permanent magnet motor modeling using magnetic equivalent circuit", *21st Iranian Conf. on Electr. Eng. (ICEE)*, pp. 1-6, Tehran, Iran (2013).

12. Gair, S., Canova, A., Eastham, J.F. and Betzer, T. "A new 2D FEM analysis of a disc machine with offset rotor", *Inter. Conf. on Power Electron., Drives and Energy Sys. for Ind. Growth - PEDES*, pp. 617-621 (1996).

13. Marignetti, F., Delli Colli, V. and Coia, Y. "Design of axial flux pm synchronous machines through 3-D coupled electromagnetic thermal and fluid-dynamical finite-element analysis", *IEEE Trans. on Ind. Electron.*, **55**(10), pp. 3591-3601 (2008).

14. Egea, A., Almandoz, G., Poza, J., Ugalde, G. and Escalada, A.J. "Axial-flux-machine modeling with the combination of FEM-2-D and analytical tools", *IEEE Trans. on Ind. Appl.*, **48**(4), pp. 1318-1326 (2012).

15. Vansompel, H., Sergeant, P. and Dupre, L. "Effect of segmentation on eddy-current loss in permanent-magnets of axial-flux PM machines using a multilayer-2D -2D coupled model", *XXth International Conf. on Electr. Mach. (ICEM)*, pp. 228-232 (2012).

16. Abbaszadeh, K., Saied, S., Hemmati, S. and Tenconi A. "Inverse transform method for magnet defect diagnosis in permanent magnet machines", *IET Electr. Power Appl.*, **8**(3), pp. 1-10 (2013).

17. Saied, S., Abbaszadeh, K., Tenconi, A. and Vaschetto, S. "New approach to cogging torque simulation using numerical functions", *IEEE Trans. on Ind. Appl.*, **50**(4), pp. 2420-2426 (2014).

18. Parviainen, A., Niemela, M. and Pyrhonen, J. "Modeling of axial flux permanent-magnet machines", *IEEE Trans. on Ind. Appl.*, **40**(5), pp. 1333-1340 (2004).

19. Azzouzi, J., Barakat, G. and Dakyo, B. "Quasi-3-D analytical modeling of the magnetic field of an axial flux permanent-magnet synchronous machine", *IEEE Trans. on Energy Convers.*, **20**(4), pp. 746-752 (2005).

20. Zhu, Z.Q. and Howe, D. "Analytical prediction of the cogging torque in radial-field permanent magnet brushless motors", *IEEE Trans. on Magn.*, **28**(2), pp. 1371-1374 (1992).

21. Chung, M.J. and Gweon, D.G. "Modeling of the armature slotting effect in the magnetic field distribution of a linear permanent magnet motor", *Electr. Eng.*, **84**(2), pp. 101-108 (2002).

22. Gholamian, S.A., Ardebili, M. and Abbaszadeh, K. "Selecting construction of high power density double-sided axial flux slotted permanent magnet motors for electric vehicles", *International Review of Electr. Eng. (IREE)*, **4**(3), pp. 477-484 (2009).

23. Gholamian, S.A., Ardebili, M., Abbaszadeh, K. and Mahmodi Charati, S. "Optimum design of 1KW axial flux permanent magnet slotted TORUS motor", *Euro. Jour. of Sci. Res.*, **21**(3), pp. 488-499 (2008).

24. Meessen, K.J., Paulides, J. and Lomonova, A.E. "Force calculations in 3-D cylindrical structures using Fourier analysis and the Maxwell stress tensor", *IEEE Trans. on Magn.*, **49**(1), pp. 536-545 (2013).

Biographies

Karim Abbaszadeh received the BS degree in Communication Engineering from Khajeh Nasir University of Technology, Tehran, Iran, in 1994, and the MS and PhD degrees in Electrical Engineering from Amir Kabir University of Technology, Tehran, Iran, in 1997 and 2000, respectively. From 2001 to 2003, he was a visiting scholar in Texas A&M University, College Station. In July 20003, he joined the Department of Electrical Engineering, K. N. Toosi University, Tehran, Iran. His main research interests and experience include analysis and design of electrical machines, fault diagnosis of electric machinery, power electronics, sensorless variable speed drives, and multiphase variable-speed drives.

Alireza Rahimi received the BS degree in Electrical Engineering from Shahrood University of Technology, Shahrood, Iran, in 2010, and the MS degree in Electrical Machines and Power Electronics from Khajeh Nasir University of Technology, Tehran, Iran, in 2013. He is pursuing his PhD degree in Electrical Engineering at the ACECR Nasir Branch, Tehran, Iran. His current research interests include PM machine modeling and EMC/EMI power electronics modeling and measurements methods.